

Ultrafast Control of the Electronic Phase of a Manganite via Mode-Selective Vibrational Excitation

M. Rini,¹ R.I. Tobey,² N. Dean,² Y. Tomioka,³ Y. Tokura,³ R. W. Schoenlein¹ & A. Cavalleri^{1,2}

¹ Lawrence Berkeley National Laboratory, 1 Cyclotron Road, MS 2-300, Berkeley, CA 94720

² Dept of Physics, Clarendon Laboratory, University of Oxford, Parks Road, Oxford OX1 3PU, UK

³ Correlated Electron Research Center, AIST Tsukuba Central 4, Tsukuba, Ibaraki, 305-8562 Japan

Controlling a phase of matter by coherently manipulating specific vibrational modes has long been an attractive and yet elusive goal for ultrafast science. Solids with strongly correlated electrons, in which even subtle crystallographic distortions can result in colossal changes of the electronic and magnetic properties, may indeed be directed between competing ground-state phases by selective vibrational excitation. In this way, new insight into the underlying physics can be gained and the dynamics in the electronic ground state of the system become accessible. Here, we report on the ultrafast switching of the electronic phase of a magnetoresistive manganite via direct excitation of a phonon mode at 17-THz. A prompt, five-order-of-magnitude drop in resistivity is observed, associated with a non-equilibrium transition from the stable insulating phase to a metastable metallic phase. In contrast with light-induced¹⁻³ and current-driven⁴ phase transitions, the vibrationally-driven bandgap collapse observed here is not related to hot-carrier injection and is uniquely attributed to a large-amplitude Mn-O distortion. This corresponds to a perturbation of the perovskite-structure tolerance factor, which controls the electronic bandwidth via inter-site orbital overlap.⁵⁻⁶ Phase control by coherent manipulation of selected metal-oxygen phonons will find extensive application in other complex solids, notably in cuprate superconductors in which the role of Cu-O vibrations on the electronic properties is controversial.

Manganites exhibit a number of exotic phenomena, including charge-ordered and striped phases, orbital and magnetic ordering, half-metallicity, phase separation and colossal magnetoresistance (CMR).⁵⁻⁶ Most of these phenomena stem from the strong interaction between lattice, charge, orbital and spin degrees of freedom, which compete on similar energy scales to determine the ground state of the system.⁷ Arguably, the most striking aspect of the physics of manganites is the occurrence of a number of metal-insulator transitions, initiated for instance via perturbations of temperature, magnetic field, pressure, and irradiation with light.

$\text{Pr}_{1-x}\text{Ca}_x\text{MnO}_3$ (PCMO) is a unique example among manganites, exhibiting insulating behavior over the entire chemical composition (x) and temperature range.⁸ This is a consequence of the small ionic radius of Ca, which results in a pronounced orthorhombic distortion (Fig. 1) that favors charge localization.⁶ Notably, the insulating phase at $x=0.3$ adjoins a “hidden” metallic state of the system, characterized by enormous changes in resistivity.

In ABO_3 perovskites, the orthorhombic distortion is quantified by the geometric “tolerance factor” that depends on the average A-O ($A=\text{Pr},\text{Ca}$) and B-O ($B=\text{Mn}$) distances:

$$\Gamma = \frac{(A - O)}{\sqrt{2}(Mn - O)}$$

where $\Gamma = 1$ corresponds to an ideal cube, while $\Gamma < 1$ reflects a compression of the Mn-O bond and an elongation of the A-O bond. Moreover, $\Gamma < 1$ indicates a Mn-O-Mn angle θ that is smaller than 180° , consistent with a symmetry-lowering rotation leading to orthorhombic or rhombohedral structures. The tolerance factor is related to the electronic properties of the solid via the one electron bandwidth (W), since the capacity for $3d$ -electrons to hop between neighboring Mn-atoms depends on a super-transfer process via $O(2p)$ states and on the degree of overlap between orbitals in neighboring sites.^{6, 9-10} The hopping matrix element is maximum at $\theta=180^\circ$ (cubic), and decreases with θ , vanishing at $\theta=90^\circ$. Systematic studies of several $\text{A}_{0.7}\text{A}'_{0.3}\text{MnO}_3$ compounds show

that the tolerance factor controls the competition between ferromagnetic metallic, paramagnetic insulating, and ferromagnetic insulating phases.¹¹

Here we show that coherent THz excitation of specific infrared-active modes can control the electronic phase of a manganite via direct modulation of the tolerance factor. Figure 1(b) shows the low-temperature optical conductivity spectrum of $\text{Pr}_{0.7}\text{Ca}_{0.3}\text{MnO}_3$ with three dominant phonon modes (23, 42, and 71 meV)¹² corresponding to the three (F_{2u}) infrared active vibrational modes of a cubic perovskite.¹³ The two highest frequency vibrations are assigned to the Mn-O-Mn bending mode and the Mn-O stretching mode respectively.¹⁴ Both vibrational modes affect the geometrical parameters determining the tolerance factor and are thus expected to have a strong coupling to the electronic properties of the system. Here we focus on the highest-frequency Mn-O stretching vibration at $17\ \mu\text{m}$ (17 THz or $580\ \text{cm}^{-1}$) and study the effect of coherent large-amplitude excitation of this mode with intense femtosecond mid-infrared pulses. The material response is investigated using both ultrafast pump-probe spectroscopy and transient conductivity measurements to characterize the insulator-metal transition.^{2-3, 15-18}

In the pump-probe spectroscopy studies, $\text{Pr}_{0.7}\text{Ca}_{0.3}\text{MnO}_3$ samples¹⁹ at 30 K are excited by 200 fs laser pulses centered at $17\ \mu\text{m}$, and the transient changes in reflectivity are measured over a broad spectral range (visible to near-infrared) in order to identify the characteristic spectral signatures and formation time of the metallic phase. Figure 2(a) shows the transient reflectivity ($\Delta R/R$) at 800 nm following impulsive vibrational excitation (at a fluence of $\sim 1\text{mJ}/\text{cm}^2$) and compared with above-bandgap pulsed excitation. The reflectivity responses are identical, with large long-lived changes in reflectivity developing within 1 ps of excitation. Moreover, these changes exhibit threshold and saturation dependence on the pump fluence, characteristic of a phase transformation to the metallic state, as previously established for *above-bandgap* excitation.¹⁶

Figure 2(b) shows the spectral dependence of the $\Delta R/R$ signal (at 1 ps delay) for the case of

17 μm pump wavelength. The spectrum of the reflectivity changes exhibits identical features as in previous optical studies in $\text{Pr}_{0.7}\text{Ca}_{0.3}\text{MnO}_3$,¹⁸ which showed that the transition to the conducting phase (induced by either applied magnetic field, or by *above-bandgap* transient optical excitation) is characterized by decreased reflectivity at photon energies in the 0.5-1.9 eV range and increased reflectivity at higher photon energies. Such reflectivity changes have been interpreted as consequence of melting of the charge order and of the collapse of the 0.3 eV insulating gap leading to the formation of a pseudo plasma edge in the metallic state.¹² Our observation of the ultrafast formation of a metallic-like reflectivity spectrum following 17 μm pump excitation provides the first evidence that the metallic state is formed promptly (within the 300 fs experimental resolution) via direct vibrational excitation,²⁰ and that this state persists for 100's of picoseconds.

Figure 2(c) shows the dependence of the reflectivity change (1 ps delay, 800 nm probe) on the pump wavelength, in the vicinity of the phonon resonance. The observed reflectivity change clearly vanishes when the pump wavelength is tuned outside the 17 μm phonon absorption band. The magnitude of $\Delta R/R$ is maximum when the excitation wavelength is resonant with the Mn-O stretching mode, providing further evidence of an ultrafast vibrationally-induced phase transition.

In addition to the optical measurements, changes in the sample conductivity are directly monitored by measuring the transient sample resistance following mid-IR excitation. Gold electrodes with a 200 μm -wide gap are deposited on the sample surface, and are DC-biased at 30 V. Measurements are performed at 30 K, where the charge-ordered, anti-ferromagnetic phase exhibits strong insulating character. Laser pulses at 17 μm are used to excite the sample (under conditions identical to those described above), with the laser spot fully covering the space between the electrodes. The current flowing through the sample was monitored by measuring the voltage drop across a 50- Ω resistor. Mid-infrared excitation results in a dramatic 1000-fold increase in current (Fig. 3, upper panel), corresponding to a resistance drop from 2 G Ω to 1.25 M Ω . The high

conductivity state develops within the 4-ns resolution of the electronics²¹ and exhibits a similar resonance behavior as observed in the optical measurements (Fig. 2c). Figure 3 shows the increase of the sample conductivity derived from the measured transient resistance by assuming that the transition to the conductive state is uniform throughout the excited sample volume. Given the laser spot size at the electrodes ($200 \times 300 \mu\text{m}^2$) and the penetration depth of the mid-infrared light ($\sim 0.5 \mu\text{m}$),¹² the sample conductivity increase is estimated to exceed 10^5 , from $\sim 3 \cdot 10^{-8} \Omega^{-1} \cdot \text{cm}^{-1}$ to $\sim 5 \cdot 10^{-3} \Omega^{-1} \cdot \text{cm}^{-1}$. In these measurements, contributions from interband carrier excitations are negligible since five photons at $17 \mu\text{m}$ (70 meV) are required to span the 0.3-eV insulating-bandgap of PCMO. The moderate temperature jump due to laser excitation (estimated at $< 2 \text{ K}$) can also be ruled out as the origin of the resistivity drop. As emphasized in the introduction, in $\text{Pr}_{0.7}\text{Ca}_{0.3}\text{MnO}_3$ an insulator-to-metal phase transition cannot be induced by temperature.⁸

Our results clearly show that resonant excitation of the Mn-O phonon vibration in $\text{Pr}_{0.7}\text{Ca}_{0.3}\text{MnO}_3$ drives the system on a femtosecond timescale into a metastable, nanosecond-lived, high-conductivity phase. It is noteworthy that this occurs in the electronic ground state of the solid and no electronic excitation is involved. These results strongly suggest that coherent modulation of the ‘tolerance factor’ gives rise to dramatic changes in the electron hopping probability, providing important new insight into the physics underlying the behavior of this strongly correlated material.

Given present limitations in generating mid-infrared pulses beyond $25 \mu\text{m}$, it is not yet possible to assess the specificity of the Mn-O stretching vibration by comparing with excitation of lower frequency phonon modes, including the Mn-O-Mn bending mode, which is also likely to significantly modulate the tolerance factor. Moreover, an important role in inducing the phase transition and subsequently stabilizing the metallic phase may be played by ultrafast vibrational energy redistribution via anharmonic coupling to the Mn-O-Mn bend, or to other modes (e.g. non infrared-active Jahn-Teller modes²²) that may also influence the electron localization and

delocalization.

Magneto-optic Kerr effect measurements following mid-infrared excitation will be important in the future to establish whether this insulator-to-metal transition is synonymous with an antiferromagnetic-to-ferromagnetic phase transformation, as would be expected for a magnetoresistive manganite where metallicity is associated with ferromagnetism through a double-exchange mechanism.²³ This implies the possibility of inducing ferromagnetic order on a sub-picosecond timescale by excitation of specific vibrational degrees of freedom, a remarkable consequence of the strong coupling between magnetic, electronic, and lattice degrees of freedom.

The excitation of a specific phonon mode has been demonstrated as a tool to drive the solid in the electronic ground state toward a competing phase of the system. The ultrafast vibrational control of correlated-electron phases is likely applicable in other interesting cases, opening a new window on their controversial physics and enabling time-resolved measurements under the unique conditions created by the initial localization of energy in specific vibrational modes. This approach may extend well beyond the case of CMR manganites, providing new insight into the behavior of complex matter, including the controversial nature of High- T_C superconductivity and the role played by lattice vibrations in determining its electronic properties.

FIGURE CAPTIONS

Figure 1: PCMO crystal structure and vibrational spectrum. (a) Unit cell of PCMO with pronounced orthorhombic distortion resulting from the small ionic radius of the Ca atoms. The Mn-O-Mn bond is bent at an angle $\theta < 180^\circ$, which varies linearly with the tolerance factor Γ .¹⁰ The Pr/Ca doping results in an alternating network of Mn^{3+} and Mn^{4+} ions. The crystal field splits the fivefold Mn-3d levels into t_{2g} and e_g subsets. The electron hopping occurs between 3d- e_g levels of neighboring Mn^{3+} and Mn^{4+} species. The lattice distortion is related monotonically to the one electron bandwidth (W), since the effective hopping interaction of 3d-electrons between neighboring Mn-sites depends on super-transfer process via O(2p) states, and the p-orbital of oxygen cannot point towards two manganese atoms simultaneously if $\theta \neq 180^\circ$.⁶ (b) Low temperature optical conductivity spectrum of PCMO. The inset shows the atomic displacements within the MnO_6 octahedra associated with the 17- μm phonon mode which modulates the Mn-O distance and hence the tolerance factor.

Figure 2: Femtosecond pump/probe reflectivity studies. (a) Relative change of reflectivity at 800 nm ($\Delta R/R$) as a function of pulse delay following vibrational excitation at 17 μm (solid line) and 800-nm photo-excitation (dotted line). (b) Spectral dependence of $\Delta R/R$ measured 1 ps after vibrational excitation. (c) $\Delta R/R$ at 800 nm measured 1 ps after excitation (squares) and absorption spectrum around the 17 μm phonon resonance (solid line). For comparison, the phonon spectrum is convolved with the spectrum of the broad-bandwidth pump pulses.

Figure 3: Time-dependent transport measurement. Vibrational excitation of the Mn-O stretching mode results in a $\sim 10^3$ increase in the sample current (upper panel) and a corresponding $\sim 10^5$ increase in the sample conductivity (lower panel). The metastable metallic phase is formed and relaxes within the

experimental time resolution of 4 ns. The dashed line ($t < 0$) shows the DC conductivity of the insulating phase. The oscillations observed at $t > 0$ are due to electronic ringing and hinder a precise assessment of the timescale for the full recovery of the insulating phase conductivity.

REFERENCES.

1. Kiriukhin, V. *et al.* An X-ray induced insulator-metal transition in a magnetoresistive manganite. *Nature* **386**, 813 (1997)
2. Miyano, K. Tanaka, T. Tomioka, Y. & Tokura, Y. Photoinduced Insulator-to-Metal Transition in a Perovskite Manganite. *Phys. Rev. Lett.* **78**, 4257 (1997)
3. Fiebig, M. Miyano, K. Tomioka, Y. & Tokura, Y. Visualization of the Local Insulator-Metal Transition in $\text{Pr}_{0.7}\text{Ca}_{0.3}\text{MnO}_3$. *Science* **280**, 1925-1928 (1998).
4. Asamitsu, A. Tomioka, Y. Kuwahara, H. & Tokura, Y. Current switching of resistive states in magnetoresistive manganites. *Nature* **388**, 50-52 (1997)
5. Tokura, Y. *Colossal magnetoresistive oxides*. (Gordon and Breach Science Publishers, 2000).
6. Dagotto, E. *Nanoscale Phase Separation and Colossal Magnetoresistance. The Physics of Manganites and Related Compounds*. (Berlin, Springer-Verlag; 2002)
7. Salamon, M.B. & Jaime, M. The physics of manganites: structure and transport. *Rev. Mod. Phys.* **73**, 583-628 (2001)
8. Tomioka, Y. Asamitsu, A. Kuwahara, H. & Moritomo, Y. Magnetic-field-induced metal-insulator phenomena in $\text{Pr}_{0.7}\text{Ca}_{0.3}\text{MnO}_3$ with controlled charge-ordering instability. *Phys. Rev. B* **53**, 1689-1692 (1996).
9. Anderson, P.W. and Hasegawa, H. Considerations on double exchange. *Phys. Rev.* **100**, 675-681 (1955).
10. Imada, M. Fujimori, A. & Tokura, Y. Metal-insulator transitions. *Rev. Mod. Phys.* **70**, 1039-1263 (1998).
11. Hwang, H.Y. Cheong, S-W. Radaelli, P.G. Marezio, M. & Batlogg, B. Lattice effects on the magnetoresistance in doped LaMnO_3 . *Phys. Rev. Lett.* **75**, 914-917 (1995).
12. Okimoto, Y. Tomioka, Y. Onose, Y. Otsuka, Y. & Tokura, Y. Optical study of $\text{Pr}_{1-x}\text{Ca}_x\text{MnO}_3$

- ($x=0.4$) in a magnetic field: Variation of electronic structure with charge ordering and disordering phase transitions. *Phys. Rev. B* **59**, 7401-7408 (1999).
13. The orthorhombic distortion is responsible for the appearance of a number weaker resonances, although only a subset of the active 25 ($7B_{1u}+9B_{2u}+9B_{3u}$) infrared phonon modes of a *Pbnm* orthorhombic structure are clearly visible.
 14. Boris, A.V. *et al.* Infrared optical properties of $\text{La}_{0.7}\text{Ca}_{0.3}\text{MnO}_3$ epitaxial films. *J. Appl. Phys.* **81**, 5756-5758 (1997).
 15. Ogawa, K. Wei, W. Miyano, K. Tomioka, Y. & Tokura, Y. Stability of a photoinduced insulator-metal transition in $\text{Pr}_{0.7}\text{Ca}_{0.3}\text{MnO}_3$. *Phys. Rev. B* **57**, R15033-R15036 (1998).
 16. Fiebig, M. Miyano, K. Tomioka, Y. & Tokura, Y. Reflection spectroscopy on the photoinduced local metallic phase of $\text{Pr}_{0.7}\text{Ca}_{0.3}\text{MnO}_3$. *Appl. Phys. Lett.* **74**, 2310-2312 (1999)
 17. Fiebig, M. Miyano, K. Satoh, T. Tomioka, Y. & Tokura, Y. Action spectra of the two-stage photoinduced insulator-metal transition in $\text{Pr}_{0.7}\text{Ca}_{0.3}\text{MnO}_3$. *Phys. Rev. B* **60** 7944-7949 (1999).
 18. Fiebig, M. Miyano, K. Tomioka, Y. & Tokura, Y. Sub-picosecond photo-induced melting of a charge-ordered state in a perovskite manganite, *Appl. Phys. B* **71**, 211-215 (2000).
 19. PCMO samples are grown via floating-zone technique and subsequently cut, polished, and annealed in an oxygen environment in preparation for pump-probe studies. The sample was excited by 1 μJ mid-infrared pulses centered at 17 μm . The pump pulses were focused on a $200\times 300 \mu\text{m}^2$ spot (to a fluence of about $1\text{mJ}/\text{cm}^2$) and the reflectivity was probed by delayed 800 nm pulses.
 20. While the spectral reflectivity signature is associated with the conducting phase of $\text{Pr}_{0.7}\text{Ca}_{0.3}\text{MnO}_3$, our recent measurements show this is not uniquely indicative of the melting of charge order, since a similar spectral signature is observed when the metallic phase is induced by photoexcitation from the room-temperature paramagnetic insulating phase [M.

Rini et al., in preparation].

21. The precise assessment of the lifetime of the metallic phase by means of transport measurements is hindered by oscillations due to spurious ringing in the fast pulse detection scheme. The sample however recovers its original resistance of $2 \text{ G}\Omega$ within several tens of nanoseconds.
22. Millis, A.J. Shraiman, B.I. & Mueller, R. Dynamic Jahn–Teller effect and colossal magnetoresistance in $\text{La}_{1-x}\text{Sr}_x\text{MnO}_3$. *Phys. Rev. Lett.* **77**, 175–178 (1996).
23. Zener, C. Interaction between the *d*-Shells in the Transition Metals. II. Ferromagnetic Compounds of Manganese with Perovskite Structure. *Phys. Rev.* **82**, 403–405 (1950).

Acknowledgements This work was supported by the Director, Office of Science, Office of Basic Energy Sciences, Materials Sciences and Engineering Division, of the U.S. Department of Energy under Contract No. DE-AC02-05CH11231. Work at the University of Oxford was supported by the European Science Foundation through a European Young Investigator Award, and by Oxford University Press through a John Fell Award.

Author information Correspondence and request for materials should be addressed to M.R. (mrini@lbl.gov) or to A. C. (a.cavalleri@physics.ox.ac.uk)

Figure 1.

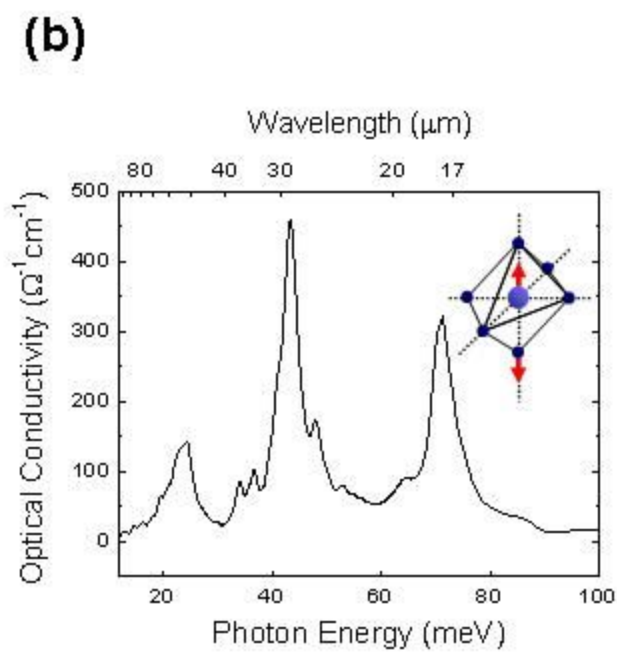
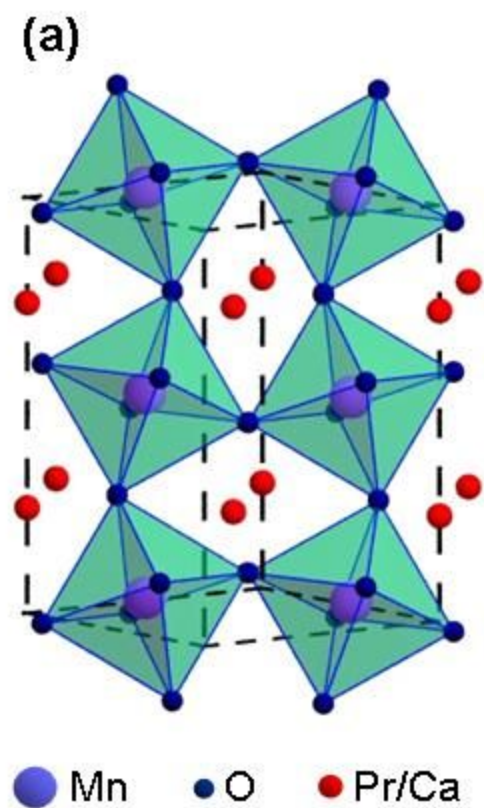


Figure 2.

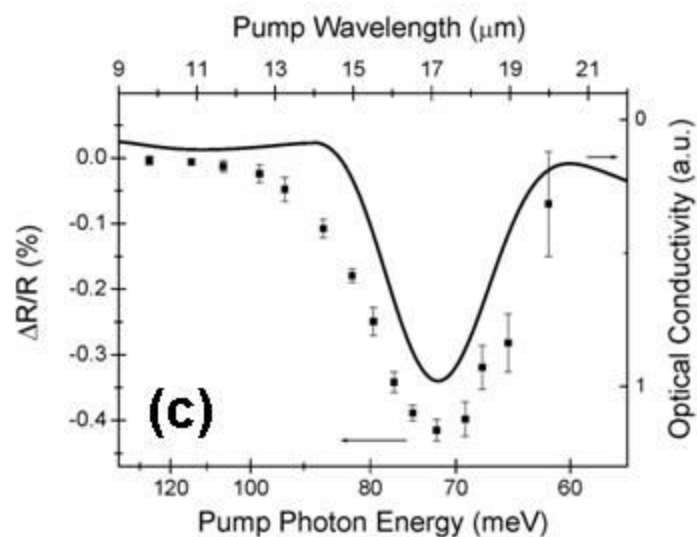
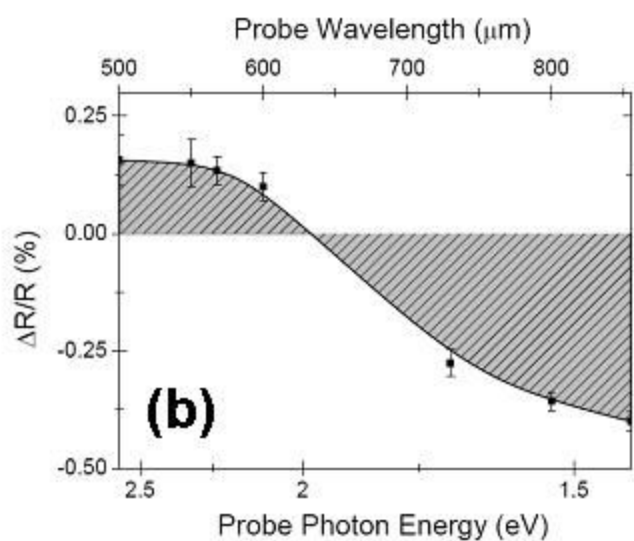
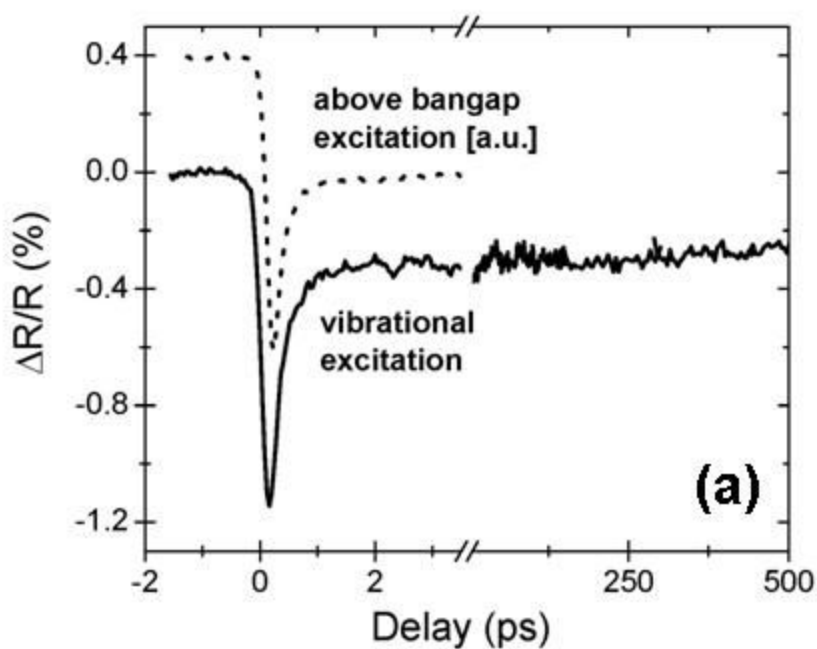


Figure 3.

